

# Pose-Free Generalizable Rendering Transformer

Zhiwen Fan<sup>1\*</sup>, Panwang Pan<sup>2\*</sup>, Peihao Wang<sup>1</sup>, Yifan Jiang<sup>1</sup>,  
 Hanwen Jiang<sup>1</sup>, Dejia Xu<sup>1</sup>, Zehao Zhu<sup>1</sup>, Dilin Wang<sup>3</sup>, Zhangyang Wang<sup>1</sup>  
<sup>1</sup>University of Texas at Austin, <sup>2</sup>ByteDance <sup>3</sup>Meta  
 {zhiwenfan, atlaswang}@utexas.edu



Figure 1. Inference pipeline of our Pose-Free Generalizable Rendering Transformer (**PF-GRT**), which facilitates novel view synthesis without the need for computing camera poses (left). We present zero-shot (generalizable) rendering results on various datasets (right).

## Abstract

In the field of novel-view synthesis, the necessity of knowing camera poses (e.g., via Structure from Motion) before rendering has been a common practice. However, the consistent acquisition of accurate camera poses remains elusive, and errors in pose extraction can adversely impact the view synthesis process. To address this challenge, we introduce **PF-GRT**, a new Pose-Free framework for Generalizable Rendering Transformer, eliminating the need for pre-computed camera poses and instead leveraging feature-matching learned directly from data. **PF-GRT** is parameterized using a local relative coordinate system, where one of the source images is set as the origin. An Omniview Transformer is designed for fusing multi-view cues under the pose-free setting, where unposed-view fusion and origin-centric aggregation are performed. The 3D point feature along target ray is sampled by projecting onto the selected origin plane. The final pixel intensities are modulated and decoded using another Transformer. **PF-GRT** demonstrates an impressive ability to generalize to new scenes that were not encountered during the training phase, without the need of pre-computing camera poses.

Our experiments with zero-shot rendering on the LLFF, RealEstate-10k, Shiny, and Blender datasets reveal that it produces superior quality in generating photo-realistic images. Moreover, it demonstrates robustness against noise in test camera poses. Code is available at [https://](https://zhiwenfan.github.io/PF-GRT/)

[zhiwenfan.github.io/PF-GRT/](https://zhiwenfan.github.io/PF-GRT/).

## 1. Introduction

Novel view synthesis, as demonstrated by recent works [22, 36, 40, 43, 48], has showcased the capability to generate new views on unseen scenes in a feed-forward manner. Despite their effectiveness, the prerequisite of camera poses for each view to offer explicit geometric priors between scene structures and 2D pixels is a common practice utilizing Structure from Motion (SfM) [33] before rendering. However, accurate camera poses not only complicate the synthesis pipeline but also restrict applicability in scenarios where precise camera information is unavailable or difficult to obtain. In some cases, inaccurate pose estimation propagates its error to the renderer, adversely reducing the synthesized image quality. One could bypass the demand for camera poses by adopting only a single image to learn generalizable NeRFs (e.g., PixelNeRF [48]), and render the target image from the constructed feature volume. On the other hand, Scene Representation Transformer (SRT)[31] and RUST[32] have pioneeringly explored the representation of multiple images as a “set latent scene representation” and generate novel views even in the presence of flawed camera poses or without any pose information. However, these works still face challenges: scene reconstruction under a single input is highly ill-posed and fails easily in in-the-wild scenes, while the latent representation results in blurred rendering outcomes with a lower res-

\*Equal Contribution.

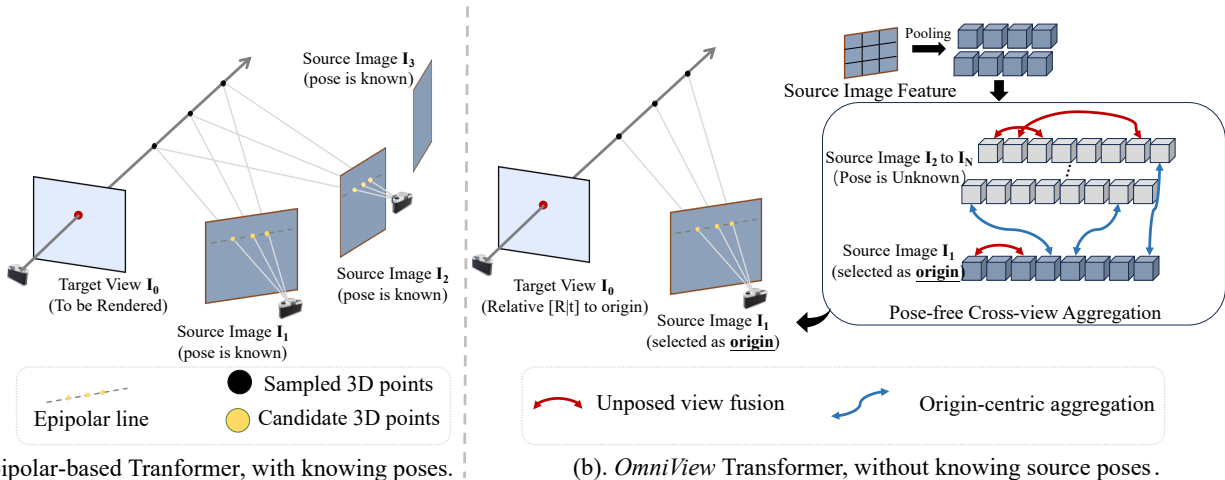


Figure 2. **Epipolar Transformer vs. OmniView Transformer.** The Epipolar Transformer requires camera poses to search for candidate matching along the epipolar line. The OmniView Transformer finds the correspondences using global feature matching by using Unposed View Fusion and Origin-Centric Aggregation, which does not rely on camera poses.

olution (e.g.,  $128 \times 128$  in SRT), limiting their applicability in achieving photorealistic rendering. In this work, we take a step forward, unifying global feature matching with Transformer [41] and the image-based rendering (IBR) [14] for **photo-realistic novel view synthesis without the need for camera poses and per-scene optimization**, all accomplished in a feed-forward pass.

Our proposed framework, PF-GRT, is parameterized by a local coordinate system, where one unposed view is used as a starting point (origin), and the target view to be rendered is defined by a relative transformation. Another key design element comes from using Transformer for global feature matching and fusing the multi-view cues: the proposed *OmniView Transformer* sequentially performs Unposed View Fusion and Origin-Centric Aggregation without the requirement of camera poses for computing epipolar constraints. Pixel-aligned 3D feature along each target ray is sampled by projecting onto the origin plane of the local system. The final pixel intensities along each target ray are modulated and decoded using another transformer, taking into account all warped 3D point features.

In training, PF-GRT is optimized using a large-scale dataset [43] with calibrated multi-view images; the starting view (origin) is randomly selected, and the ground-truth poses are converted into relative for applying the photometric losses. In inference, our method selects any unposed source image as origin (the root of relative coordinate system), and can render any free-view by specifying a relative transformation relative to the origin. This is achieved without the pre-computed poses in an unseen scene.

Comprehensive experiments on diverse real-world scenes, including LLFF, RealEstate10K, Shiny, and object-level Blender datasets demonstrate our approach achieves

superior zero-shot rendering quality (see Figure 1), surpassing prior pose-free generalizable NeRFs with a large-margin. Additionally, our method demonstrates superior robustness against camera pose noise in new scenes.

Our major contributions are encapsulated as follows:

- We introduce a new formulation for generating novel views, by unifying the pixel-aligned feature of the target pixel with Image-based Rendering (IBR), eliminating the need for pose annotations among test scenes, and streamlining the rendering process.
- We propose an efficient *OmniView Transformer* to aggregate multi-view features with adaptive weights, by broadening the epipolar constraint to encompass all source pixels. A source-conditioned modulation layer is integrated to handle projection occlusions, and pixel intensities are decoded by another Transformer.
- Trained with large-scale multi-view datasets, PF-GRT is able to render photo-realistic novel views in unseen scenes in a feed-forward pass. It significantly outperforms other pose-free, generalizable neural rendering techniques in diverse datasets.

## 2. Related Works

**Generalizable Neural Scene Representations** Building generalizable feature volumes dates back to Neural Volumes [23], wherein an encoder-decoder framework is adopted to create a feature volume. Later on, NeRF [26] and its follow-ups [1–3, 9, 11, 12, 15, 16, 21, 27, 29, 34, 38, 42, 47] have emerged as effective scene representations. However, their costly per-scene fitting nature constitutes a significant limitation. Generalizable NeRFs endeavor to circumvent time-consuming optimization by conceptualizing novel view synthesis as a cross-view image-based in-

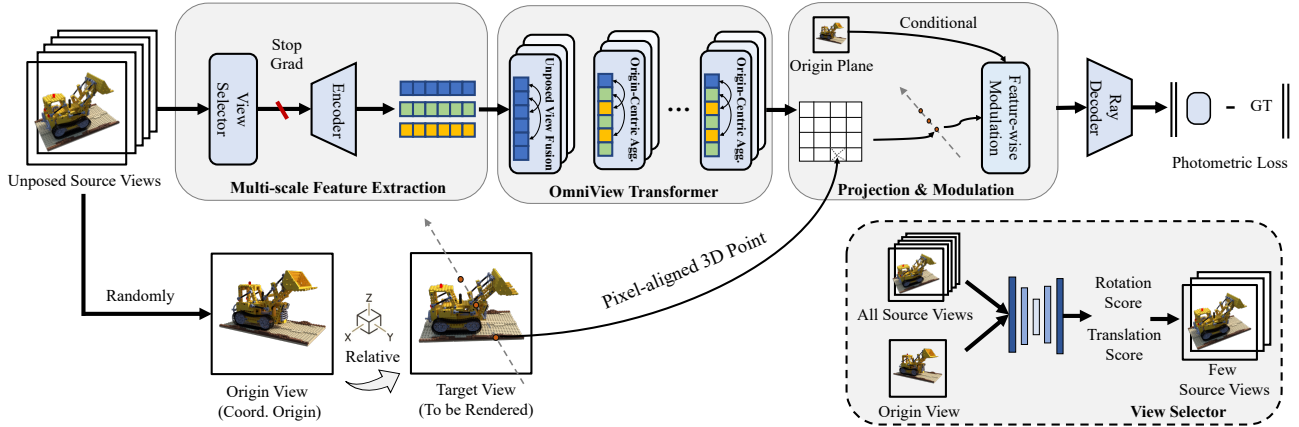


Figure 3. **The overall pipeline of the proposed PF-GRT.** Given unposed source images with a specified *origin view*, PF-GRT selects a limited number of source images closest to the origin view. Multi-scale 2D features are extracted, and the *OmniView Transformer* is used for aggregating features from the unposed sources towards the origin plane. The 3D point feature on the target ray is initialized via projection, and the final pixel intensities are modulated and then decoded using another Transformer.

terpolation problem. NeuRay [22], IBRNet [43], MVS-NeRF [5], and PixelNeRF [48] assemble a generalizable 3D representation using features aggregated from observed views. GPNR [36] and GNT [40] enhance the novel view renderings with a Transformer-based aggregation process. A view transformer aggregates image features along epipolar lines, while a ray transformer combines coordinate-wise point features along rays through the attention mechanism.

**Pose-free NeRFs** Numerous efforts have been exerted to diminish the necessity for calibrated camera poses during NeRF training. NeRF- - [44] makes an early endeavor to optimize camera parameters with NeRF training for forward-facing scenes simultaneously. BARF [19] refines NeRFs from imperfect (or even unknown) camera poses via coarse-to-fine registration, while GARF [6] incorporates Gaussian activations. NoPe-NeRF [4] employs monocular depth priors to restrict the relative poses between consecutive frames. Efforts have also been made to expand generalizable NeRF toward unposed images. PixelNeRF [48] builds a generalizable feature volume that estimates novel views from single-view observation, which can be unposed. MonoNeRF [39], when provided with a video sequence, explicitly estimates the depth maps, camera poses, along with a reconstruction loss between the rendered frames for training. FlowCam [35] explicitly estimates the camera pose of the video frame by fitting a 3D scene flow field with the assistance of a pretrained 2D optical flows model. Generalizable methods, SRT [31] and RUST [32], infer a set-latent scene representation from a set of unposed images to synthesize novel views. The concurrent work, Leap [17], constructs neural volume with feature aggregation, designed for pose-free object-level novel view synthesis.

**Transformers as Neural Scene Representations** Transformers are extensively utilized to represent scenes. IBRNet [43] processes points sampled from rays using MLP and estimates density via a transformer. NeRFormer [30] employs attention modules to craft feature volumes with epipolar geometry constraints. LFNR [37], GPNR [36] and GNT [40] introduces a two-stage transformer-based model to accumulate features along epipolar lines and aggregate features along reference views to produce the color of target rays. SRT [31] and RUST [32] infer a set-latent scene representation via a vision transformer and parameterize light fields by attending into the scene representation for novel view renderings.

### 3. Method

**Overview** Given an unposed image set with known intrinsics  $\{(\mathbf{I}_i \in \mathbb{R}^{H \times W \times 3}, \mathbf{K}_i \in \mathbb{R}^{3 \times 3})\}_{i=0}^N$  of a scene, PF-GRT synthesizes new views in a single forward pass. Specifically, the relative coordinate system is constructed with one unposed view as the origin, and the target view is defined using relative transformation. The *OmniView Transformer* performs Unposed View Fusion and Origin-Centric Aggregation towards the origin view. Pixel-aligned 3D point feature on the target ray is initialized by projecting onto the origin plane. The pixel intensities are subsequently modulated, conditioned on the origin plane, and decoded using another Transformer. To determine the most suitable source views for aggregation, a view selector is designed to identify the closest  $K$  views ( $K \leq N$ ) relative to the origin view, based on global feature distances. An overview of our pipeline is illustrated in Figure 3.

### 3.1. OmniView Transformer

We propose to use Transformer for learning global feature matching across unposed source views to find the best matching feature for rendering a target ray.

**Unposed View Fusion** Having extracted the multi-view feature from a shared 2D encoder, tokens are initialized by subdividing the feature map into  $M \times M$  patch grids, which enables generalization to various datasets under different resolutions. The Unposed View Fusion (UVF) module aggregates the features from each unposed view to capture long-range global context. Specifically, the UVF layer performs self-attention on the token set  $\mathcal{F} \in \{\mathbf{f}^1, \dots, \mathbf{f}^{M \times M}\}$  of each unposed source view, which consists of  $M \times M$  discrete tokens:

$$\mathcal{F} = \text{FFN}(\text{Attention}(\mathcal{F}, \mathcal{F})) \quad (1)$$

Here, we utilize attention layers to retrieve relevant information within the given view and update the view-specific feature to be embedded with global context information.

**Origin-Centric Aggregation** Next, we propose propagating the multi-view cue from unposed views toward the origin view ( $\mathbf{I}_0$ ), which acts as the root of the constructed local coordinate system for rendering. The proposed Origin-Centric Aggregation (OCA) performs the propagation sequentially for each source view via:

$$\mathcal{F}_0 = \text{FFN}(\text{Attention}(\mathcal{F}_0, \mathcal{F}_i)), \quad i \in N \quad (2)$$

The amalgamation of source features toward the origin view enriches the multi-view information in the updated origin feature plane. The pseudocode implementation of the OmniView Transformer is provided in the Appendix.

### 3.2. Target Ray Initialization and Decoding

To render a pixel  $\mathbf{c} = (\mathbf{o}, \mathbf{d})$  in target view, the relative transformation from origin plane is specified. Pixel-aligned 3D points  $\mathbf{p} \in \{p_1, p_2, \dots, p_M\}$  are uniformly sampled between the near and far plane. Point feature are tokenized, modulated and decoded into pixel intensities.

**Tokenizing 3D Points on Target Ray** The uniformly sampled points,  $\mathbf{p}$  are projected onto the feature maps of the origin view, culminating in the initialized point features:

$$\hat{\mathbf{p}} = \mathbf{K}_0(\mathbf{R}_0(\mathbf{p}) + t_0) \quad (3)$$

$$\mathbf{F}(\mathcal{F}_0, \hat{\mathbf{p}}) = \text{Interpolation}(\Pi(\hat{\mathbf{p}}, \mathcal{F}_0)) \quad (4)$$

Here,  $\mathbf{R}_0$  and  $t_0$  symbolize the relative rotation and translation between the target view to the origin view,  $\Pi$  represents the projection function, and  $\mathcal{F}_0$  is the extracted feature maps on origin view, formulating the pixel-aligned 3D point-wise feature  $\hat{\mathbf{p}} \in \{\hat{p}_1, \hat{p}_2, \dots, \hat{p}_M\}$ .

**Origin-Conditioned Modulation Layer** When projecting points into regions of the scene that are obscured from the camera’s viewpoint, or where erroneous feature matchings from unposed source views occur, the projected points often become occluded or missed, degrading the rendered quality. To counteract this issue, an origin view-conditioned layer is introduced to modulate the point features through an affine transformation, utilizing the extracted global coherence derived from the origin view. Formally, a Feature-wise Linear Modulation (FiLM) layer [28] is utilized to scale and shift the point feature  $\hat{\mathbf{p}}$  following:

$$\gamma^\tau, \beta^\tau = \text{MLP}_\gamma(\text{GAP}(\mathcal{F}_0)), \text{MLP}_\beta(\text{GAP}(\mathcal{F}_0)) \quad (5)$$

$$\hat{\mathbf{p}} := \gamma^\tau \hat{\mathbf{p}} + \beta^\tau \quad (6)$$

This modulation is formulated by two groups of parameters,  $\gamma^\tau$  and  $\beta^\tau$ , resulting in the modulated point-wise feature  $\hat{\mathbf{p}}$ . GAP denotes Global Average Pooling.

**Ray-based Rendering with Transformers** Recent research advocates the utilization of the Transformer architecture to adaptively learn the blending weights along the ray for each point, augmenting both expressiveness [40] and generalization [36]. Instead of using the simplified version of volume rendering [24] from NeRF [26], we employ such an “attention” mechanism to determine the aggregation weights for each sampled point feature in a data-driven way, to decode the final pixel intensity:

$$\mathbf{c}(\mathbf{o}, \mathbf{d}) = \text{MLP} \circ \text{Mean} \circ \text{Attention}(\hat{\mathbf{p}}, \hat{\mathbf{p}}), \quad (7)$$

### 3.3. View Selection via Feature Similarity

View selection aims to select efficiently a few source images, which is the nearest to the origin view, to reduce the computational redundancy when performing OmniView attention. Specifically, a network is designed to extract multi-scale features [13] from all source images, and multiple decoding heads are devised for regressing the relative rotation and translation scores between  $\mathbf{I}_0$  and each source image  $\{\mathbf{I}_i, i \neq 0\}$ . In particular, four decoding heads are utilized for estimating the three normalized relative angles and the distance value between the two images. Top  $K$  images are selected out of the  $N$  ( $K \leq N$ ).

### 3.4. Training and Inference

During the training phase, the view selector identifies the nearest  $K$  source images from the  $N$  unposed source images. This selection procedure is guided by a specified loss function that operates based on the online-computed relative angle and distance values of each image pair.

$$\Theta_s^* = \arg \min_{\Theta} (\|\angle(\mathbf{I}_0, \mathbf{I}_i) - \angle_{gt}\|_2^2 + \|d(\mathbf{I}_0, \mathbf{I}_i) - d_{gt}\|_2^2). \quad (8)$$

Methods	Real Forward-facing(LLFF)			RealEstate10K Datasets			Shiny Datasets			NeRF Synthetic Objects		
	PSNR $\uparrow$	SSIM $\uparrow$	LPIPS $\downarrow$	PSNR $\uparrow$	SSIM $\uparrow$	LPIPS $\downarrow$	PSNR $\uparrow$	SSIM $\uparrow$	LPIPS $\downarrow$	PSNR $\uparrow$	SSIM $\uparrow$	LPIPS $\downarrow$
PixelNeRF [48]	8.379	0.313	0.643	9.008	0.407	0.503	9.025	0.285	0.607	7.105	0.565	0.413
PixelNeRF-ft	10.234	0.346	0.593	11.115	0.462	0.470	10.130	0.304	0.555	7.561	0.569	0.406
UpSRT [31]	16.669	0.541	0.418	16.833	0.593	0.314	15.117	0.471	0.428	15.725	0.814	0.205
LEAP [17]	9.220	0.228	0.694	11.336	0.527	0.459	9.659	0.257	0.668	18.020	0.831	0.187
Ours	22.728	0.778	0.180	24.208	0.789	0.190	19.192	0.604	0.338	22.832	0.835	0.134

Table 1. **Quantitative Comparison in a Generalizable Pose-Free Setting.** PF-GRT outperforms previous pose-free methods that utilize both single-view feature volume (PixelNeRF)[48] and multi-view “set of latents”(UpSRT)[31], in addition to aggregation to neural volume (LEAP) [17]. Owing to the effective *OmniView Transformer* and the *IBR* formulation, our method can generate novel views with the highest quality. We color each row as **best**, **second best**, and **third best**.

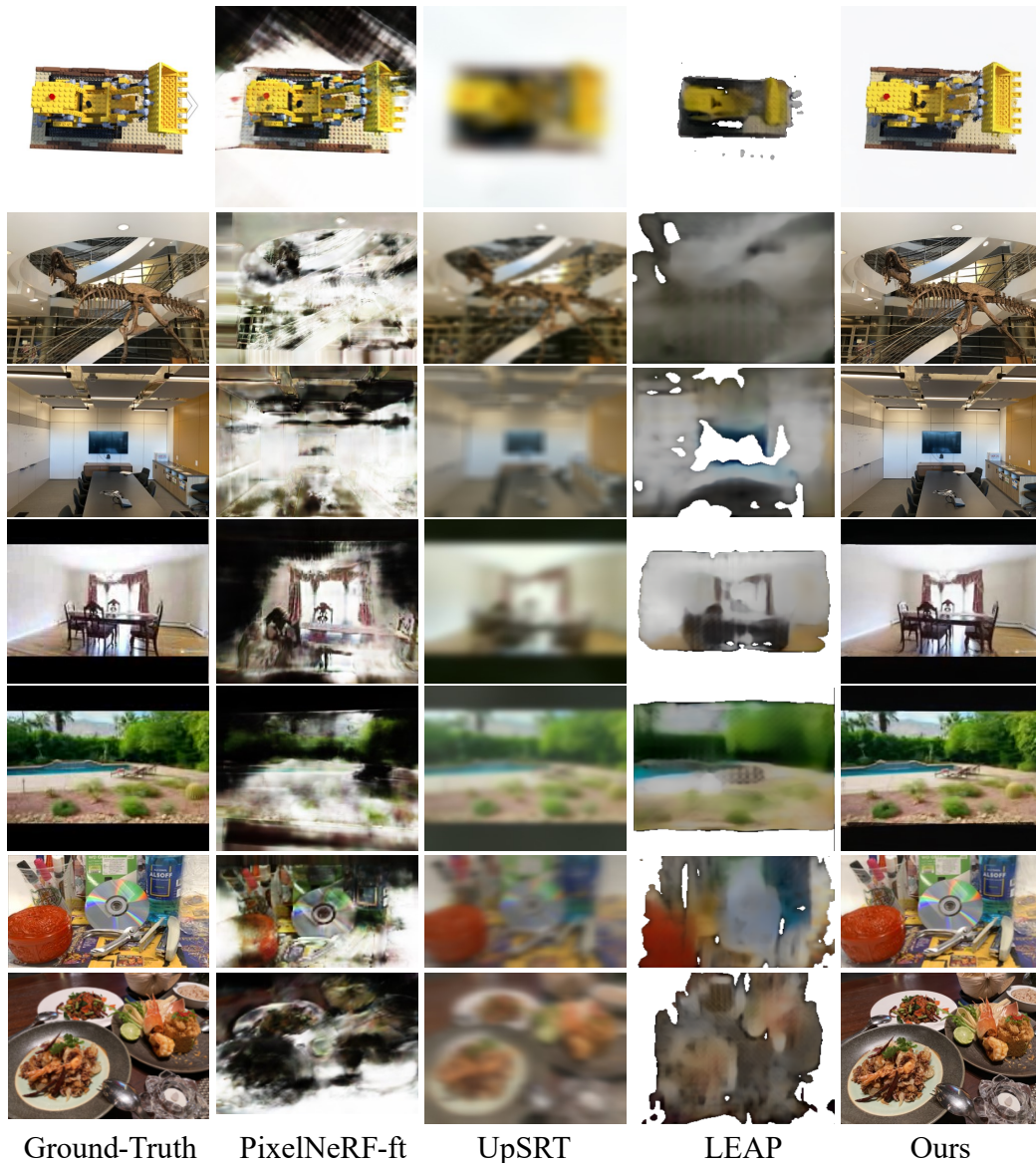


Figure 4. **Qualitative Comparison Under a Generalizable Pose-Free Setting.** Single-view PixelNeRF [48] introduces artifacts within the constructed feature volume and shows limited capacity in handling complex scenes. Multi-view SRT [31] fails to render sharp details in scenes with rich textures. LEAP [17] can generalize to object-level datasets, but it fails to scale up to scene-level synthesis. In contrast, our method more accurately recovers fine details through global correspondence matching and image-based rendering.

The rest part of the model is optimized utilizing the  $\mathcal{L}_2$  distance between the rendered target pixels and the corresponding ground-truth pixels, as exemplified by:

$$\Theta_t^* = \arg \min_{\Theta} \|C(r_i | \Theta, \theta, \mathbf{x}) - C_{gt}\|_2^2. \quad (9)$$

Note that the training requires ground-truth camera poses for calculating the score for the view selector, and the absolute poses are converted into relative poses for supervising the model training. For inference on unseen scenes, there is no reliance on any pose estimator. Instead, target views are specified based on a relative transformation from the origin view, which can be selected arbitrarily. Other source views are determined by the view selector.

## 4. Experiments

### 4.1. Implementation Details

**Datasets.** We train PF-GRT on a large-scale dataset, spanning from  $\sim 1000$  Google Scanned Objects [8] to real-world datasets: sparsely-sampled RealEstate10K [50], 100 scenes from the Spaces datasets [10], and 102 real-world scenes captured using handheld phones [25, 43]. We evaluate the zero-shot accuracy on diverse datasets without finetuning:

- **LLFF Datasets**[25] contain eight real-world forward-facing scenes, with a resolution of  $504 \times 378$ .
- **RealEstate10K**[50]. The test set consists of four real-world scenes at a resolution of  $176 \times 144$ .
- **Shiny Datasets**[45] contain eight scenes with challenging lighting conditions, with evaluations conducted on  $8 \times$  downsampled images.
- **Blender Datasets**, the widely-adopted synthetic data created by NeRF[26], encompasses eight objects with a tested resolution of  $400 \times 400$ .

**Training and Inference Details.** PF-GRT is trained end-to-end, with the gradient stopping operation after the view selector. The Adam optimizer is employed to minimize the training loss for the model. The learning rate decreases exponentially over training steps with a base of  $10^{-3}$ . The comprehensive training encompasses 250,000 steps, with 4,096 randomly sampled rays during each iteration. In both training and inference phases, 128 points are uniformly sampled along each target ray. Grid number  $M$  is set as 7 to balance efficiency and accuracy.

**Baselines.** We evaluate pose-free novel view synthesis with UpSRT [31], single-view based PixelNeRF [48], and the generalizable LEAP [17]. We re-trained UpSRT [31]<sup>1</sup> on the same datasets as ours for 400K iterations until fully converged. We report both the vanilla PixelNeRF from their provided checkpoint, and the finetuned version on the same dataset as ours. We use the checkpoint from LEAP[17]

<sup>1</sup><https://github.com/stelzner/srt>

trained on OmniObject datasets [46]. We also test robustness against camera pose noises in source views with other generalizable NeRFs [22, 40, 43]: we synthetically perturb the camera poses with additive Gaussian noise on both rotation and translation vectors, akin to BARF [19].

**Metrics** The rendering quality is reported using metrics such as peak signal-to-noise ratio (PSNR), structural similarity (SSIM), and perceptual similarity via LPIPS [49].

### 4.2. Generalizable Pose-free Novel View Synthesis.

Table 1 showcases that PF-GRT surpasses the best-performing multi-view pose-free SRT [31], LEAP [17], and single-view PixelNeRF on all unseen test scenes, encompassing synthetic datasets, forward-facing datasets, RealEstate10K datasets and Shiny datasets with complex lighting conditions. This validates the efficacy of the designed OmniView Transformer for effective view aggregation under pose-free setting, and the image-based rendering to generate detailed textures. We present qualitative results in Figure 4, wherein it can be observed that the “latent” representation in SRT overlooks the image details, and PixelNeRF struggles under complex scenes using single-view feature volume-based neural rendering. LEAP has difficulties to generalize to scene-level test cases. See the video in supplementary materials for detailed comparisons.

### 4.3. Robustness against Noisy Poses.

Multi-view images captured in the real world typically require a pre-processing step (e.g., COLMAP [33]) to compute the poses. However, this computation is slow, especially when the number of source images is large, and often contains errors [19]. We examine the current best-performing generalizable NeRFs against noisy camera poses in the tested source views, a practical concern. Following [19], who apply additive Gaussian perturbation at different levels to the camera poses, we directly test the trained generalizable model with the provided checkpoint to assess robustness. It is evident from Figure 5 that all generalizable methods suffer from noisy camera poses, with significant degradation in performance even under a small amount of noisy calibration ( $\sigma=0.003$ ). On the other hand, our framework PF-GRT, which generates new views in a feed-forward pass without estimating camera poses, demonstrates stability in rendering quality. This stability is attributed to our approach of not relying on absolute camera poses for cross-view feature aggregation but instead learning the cross-view feature mapping from large-scale training using the OmniView Transformer. Consequently, the source view pose noises do not affect the rendering quality.

Figure 6 visualizes the effect of different noise levels on source views in the evaluation, illustrating that subtle noise significantly decreases the rendering quality. Quantitative

Methods	Real Forward-facing(LLFF)			NeRF Synthetic Objects		
	PSNR $\uparrow$	SSIM $\uparrow$	LPIPS $\downarrow$	PSNR $\uparrow$	SSIM $\uparrow$	LPIPS $\uparrow$
IBRNet [43]	21.395	0.686	0.303	20.027	0.813	0.145
NeuRay [22]	21.520	0.681	0.303	21.424	0.832	0.135
GNT [40]	21.341	0.682	0.307	20.554	0.830	0.139
Ours	22.728	0.778	0.180	22.832	0.835	0.134

Table 2. **Quantitative Comparison of Robustness to Noisy Poses in source views.** The table presents a performance comparison between PF-GRT and various generalizable NeRFs using the NeRF-Synthetic [26] and LLFF datasets [25], where both rotation and translation matrices are perturbed with  $\sigma = 0.003$ . PF-GRT showcases its robustness in handling pose perturbations in rendered views. We color each row as **best**, **second best**, and **third best**.

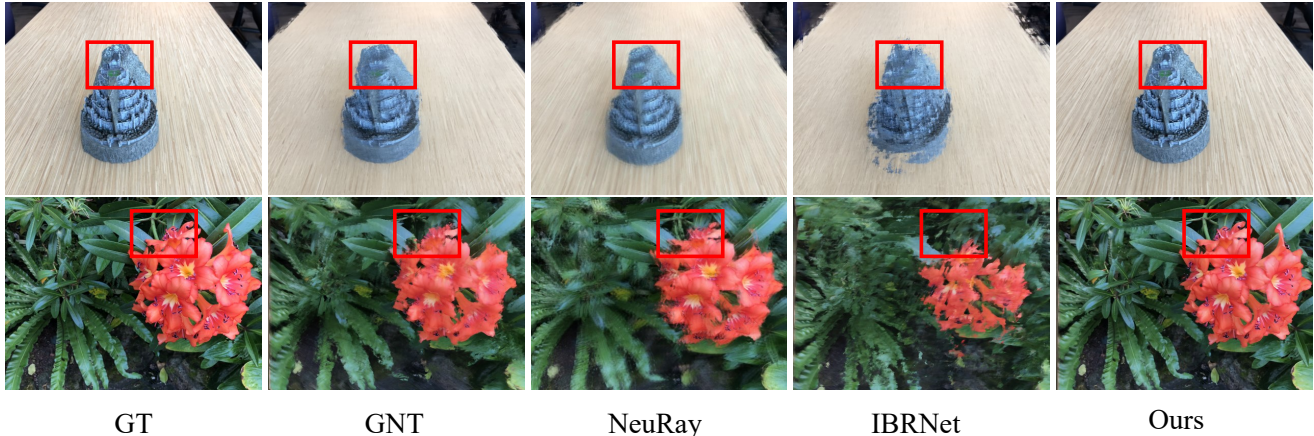


Figure 5. **Visualizations of Different Methods Against Noisy Poses on Source Images When Rendering.** All adopted generalizable NeRFs suffer from noisy camera poses in source views at evaluation, even with very mild perturbation (e.g.,  $\sigma=0.003$ ).

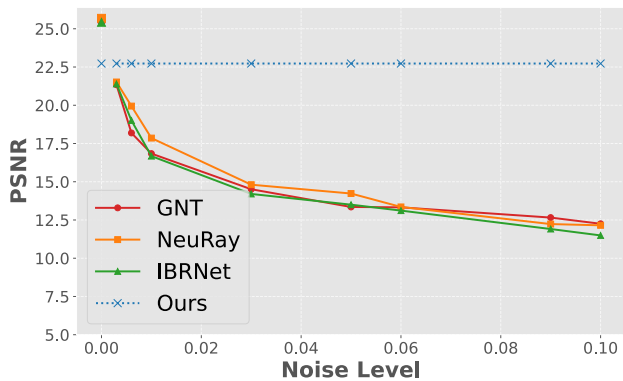


Figure 6. **Visualizations of generalizable NeRFs with different noise level.** We increases the noise from ( $\sigma=0.003$ ) to ( $\sigma=0.1$ ), methods that rely on camera poses for cross-view aggregation are decreasing in rendering quality. Our method demonstrates the robustness against test pose noises, as we perform global feature matching toward the origin view, instead of using epipolar constraints.

results, with a noise level of 0.003 on both real forward-facing and synthetic objects datasets, are presented in Ta-

ble 2.

#### 4.4. Ablation Study

We now execute a series of ablation studies regarding our module choice on the LLFF datasets [25] and average the metrics across all scenes. The evaluation begins with the use of the “origin view” directly for evaluation, and subsequently, we incrementally integrate the proposed techniques (*Pixel-aligned Feature*, *OmniView Transformer*, *Conditional Modulation Layer*) in this study.

**Pixel-aligned Feature?** We study utilizing the relative coordinate system between the origin view and the target views, and obtain the 3D point feature along the target ray by directly projecting onto origin feature plane. The final pixel intensities of target ray are regressed using ray attention. As we can see in the second row of Table 3 and the third column of Figure 7, the missing of multi-view cues results in an inferior rendering quality.

**OmniView Transformer?** We further employ the *OmniView Transformer* for Unposed-View Fusion and Origin-Centric Aggregation, using a data-driven attention mechanism focused on the origin view. This design significantly improves quantitative metrics, with an increase in PSNR

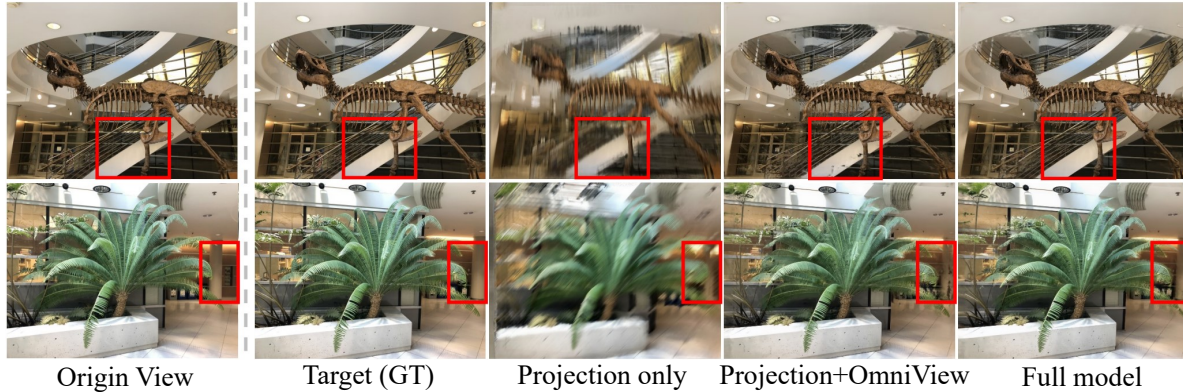


Figure 7. **Visualization for Ablation Study.** We visualize the “origin view” (1st column), “ground-truth target view” (2nd column), rendered images using projection and ray attention (3rd column), the incorporation of the *OmniView Transformer* (4th column), and our full model (last column).

Pixel-aligned Feature	OmniView Transformer	Modulation FiLM-Layer	PSNR $\uparrow$	SSIM $\uparrow$	LPIPS $\downarrow$
$\times$	$\times$	$\times$	14.198	0.355	0.407
$\checkmark$	$\times$	$\times$	16.519	0.412	0.400
$\checkmark$	$\checkmark$	$\times$	22.287	0.740	0.197
$\checkmark$	$\checkmark$	$\checkmark$	<b>22.728</b>	<b>0.778</b>	<b>0.180</b>

Table 3. **Ablation study of the proposed components in PF-GRT.** We start by constructing the relative coordinate system between origin and target view, utilizing pixel-aligned feature (2nd row) shows a better metrics than the baseline that directly evaluating the origin view (1st row). The introduction of *OmniView Transformer* (3rd row) significantly improve the PSNR from 16.519dB to 22.287dB. Additionally, the feature-wise modulation layer further improve the PSNR to 22.728dB (last row).

Random?/GT?/ View Selector?	Disentangled Decoder Heads	PSNR $\uparrow$	SSIM $\uparrow$	LPIPS $\downarrow$	Select Acc. $\uparrow$
Random	N/A	17.841	0.505	0.390	0.017
View Selector	$\times$	22.243	0.756	0.198	0.688
View Selector	$\checkmark$	22.728	0.778	0.180	0.731
GT	N/A	24.275	0.822	0.135	1.000

Table 4. **Ablation on the View Selector.** The incorporation of the view selector finds the best matched source images, enabling PF-GRT to effectively aggregate cross-view features. The employment of disentangled decoder heads for each axis of rotation and translation vector further improves the view selection accuracy and, thus, the synthesis quality. PF-GRT, which utilizes ground-truth poses for view selection, is listed in the last row.

from 16.519 to 22.287, as shown in the third row of Table 3. Additionally, Figure 7 demonstrates that the visual quality is also improved by integrating missing information from other source views.

**Conditional Modulation Layer?** Conditioned on the statistics of the origin view, the 3D point-wise features on the target ray are affine-transformed using learnable parameters. This adjustment aids in filling in missing regions in

occluded areas (see the second-last column of Figure 7) especially when cross-view aggregation is imprecise and the modulation layer can guide the projection toward a plausible solution. The last row of Table 3 shows that the modulation layer improves SSIM from 0.74 to 0.778.

**Analysis on the Viewpoint Selector.** Initially, we assess the use of random source view selection in the evaluation, where the selected source views may not be ideal for feature aggregation, resulting in a 0.505 SSIM metric (1st row of Table 4). Utilizing the selector to regress the averaged relative viewing direction and distance directly elevates the SSIM to 0.756, a significant improvement. Employing separate decoder heads to disentangle the similarity score for the three axes of relative rotation and translation distance further enhances the quantitative metrics to 0.778 ( $\uparrow 0.02$  in SSIM). Additionally, we illustrate the use of ground-truth poses to identify the nearest source views with viewing directions most analogous to the “origin view,” serving as the upper bound of the view selector.

## 5. Conclusion

We present a novel framework, PF-GRT, for photo-realistic rendering from a sparse set of unposed images. PF-GRT constructs a relative coordinate system to parameterize the target view. It adapts the *OmniView Transformer* for a pose-free setting, effectively fusing the unposed source images, and aggregating multi-view cues toward the origin view via a data-driven attention mechanism. PF-GRT enjoys the advantages of global feature matching, and Image-Based Rendering (IBR) to produce state-of-the-art rendering quality in complex scenes. Moreover, PF-GRT can render new views on unseen datasets without any scene-specific optimization and pre-computed camera poses, showcasing both the flexibility in pose annotations and robustness against noisy computed camera poses.

# Pose-Free Generalizable Rendering Transformer

## Supplementary Material

### A6. Motivation of OmniView Transformer

As previously mentioned in the main paper, knowing the multi-view camera poses enables the framework design to search for correspondences along the epipolar line. As illustrated in Figure A8(a), we consider a simple case with several source views. For the pixel to be rendered in the target view, epipolar attention used in [36, 40] builds correspondences among the target ray and epipolar line of neighboring source images. However, without knowing the poses, we are unable to build such a search pattern, and thereby, we resort to utilizing an attention mechanism to search over all source pixels toward the origin view (the relative coordinate system is constructed), which is the origin of the relative coordinate system. We propose the use of a CNN network to extract multi-scale feature maps. Subsequent to the CNN encoder, these extracted feature maps from source views ( $\mathbf{I}_i \in \mathbb{R}^{H \times W \times 3}$ ) $_{i=0}^K$  are subdivided into  $M \times M$  grids within each view, facilitating the model to be agnostic to diverse image resolutions (as shown in Figure A8 (b)). The *Unposed View Fusion*, which performs intra-image long-range global context aggregation, is designed to retrieve relevant information within the source views, while the *Origin-Centric Aggregation* focuses on capturing cross-relationships across these two views. This way, inter-image feature interaction between images is facilitated.

### A7. Implementation Details

**Memory-Efficient OmniView Transformer** The most straightforward method for aggregating the initially projected 3D point feature involves building cross-attention between the target 3D point feature and all source pixels. However, this approach is intractable as it cannot scale to high-resolution input images and a large number of source views. Therefore, we propose to leverage the  $8 \times$  downsampled CNN features and pool them into a fixed number of 2D grids (here, we use a  $7 \times 7$  grid) for each view. Consequently, our design is agnostic to input resolution, allowing attention to be performed in a patch-wise manner. Nevertheless, during training, the sampled ray is typically large (e.g., 4096 in PF-GRT), incurring  $4096 \times 128$  sampled points in each iteration. The cross-attention among sampled points and tokenized patches in the source views remains intractable. Therefore, akin to the [CLS] token in Vision Transformer [7], we employ the cross-attention mechanism to propagate multi-view information in source views toward the origin view. We then project the sampled 3D points onto the starting view, ensuring an efficient implementation regardless of the number of source views used. Please refer

to the PyTorch-like pseudo-code Algorithm 1 for a detailed explanation.

---

**Algorithm 1** OmniView Transformer: PyTorch-like Pseudo-code

---

```
 $\mathbf{p}_t \rightarrow$  points coordinate in target view( $N_{\text{rays}}, N_{\text{pts}}, 3$ )  
 $\mathbf{X}_0 \rightarrow$  flattened tokens in origin( $1, N_{\text{patch}}, C$ )  
 $\{\mathbf{X}_i\}_{i=1}^K \rightarrow$  flattened tokens in source views( $K, N_{\text{patch}}, C$ )  
 $\mathbf{f}_t \rightarrow$  projected points feature( $N_{\text{rays}}, N_{\text{pts}}, D$ )  
 $f_Q, f_K, f_V, f_{\text{rgb}} \rightarrow$  functions that parameterize MLP layers
```

```
for  $0 \leq i \leq K$  do                                ▷ Unposed View Fusion  
   $\mathbf{Q} = f_Q(\mathbf{X}_i)$   
   $\mathbf{K} = f_K(\mathbf{X}_i)$   
   $\mathbf{V} = f_V(\mathbf{X}_i)$   
   $\mathbf{A} = \text{matmul}(\mathbf{Q}, \mathbf{K}^T) / \sqrt{D}$   
   $\mathbf{A} = \text{softmax}(\mathbf{A}, \text{dim} = -1)$   
   $\mathbf{X}_i = \text{matmul}(\mathbf{A}, \mathbf{V})$   
end for
```

```
for  $1 \leq i \leq K$  do                                ▷ Origin-Centric Aggregation  
   $\mathbf{Q} = f_Q(\mathbf{X}_i)$   
   $\mathbf{K} = f_K(\mathbf{X}_0)$   
   $\mathbf{V} = f_V(\mathbf{X}_0)$   
   $\mathbf{A} = \text{matmul}(\mathbf{Q}, \mathbf{K}^T) / \sqrt{D}$   
   $\mathbf{A} = \text{softmax}(\mathbf{A}, \text{dim} = -1)$   
   $\mathbf{X}_0 = \text{matmul}(\mathbf{A}, \mathbf{V})$   
end for
```

```
for  $0 \leq i \leq (N_{\text{rays}} \times N_{\text{pts}})$  do                ▷ Point-wise projection  
   $\mathbf{f}_t^i = \text{interp}(\text{proj}(\text{modulation}(\mathbf{p}_t^i), \mathbf{X}_0))$   
end for
```

```
for  $0 \leq i \leq N_{\text{rays}}$  do                            ▷ Ray attention  
   $\mathbf{Q} = f_Q(\mathbf{f}_t^i)$   
   $\mathbf{K} = f_K(\mathbf{f}_t^i)$   
   $\mathbf{V} = f_V(\mathbf{f}_t^i)$   
   $\mathbf{A} = \text{matmul}(\mathbf{Q}, \mathbf{K}^T) / \sqrt{D}$   
   $\mathbf{A} = \text{softmax}(\mathbf{A}, \text{dim} = -1)$   
   $\mathbf{f}_t^i = \text{matmul}(\mathbf{A}, \mathbf{V})$   
end for
```

```
RGB =  $f_{\text{rgb}}(\text{mean}_{i=1}^{N_{\text{pts}}}(\mathbf{f}_t^i))$ 
```

---

### A8. Additional Experiments

**Scene-wise Quantitative Metrics** Table A5, Table A6 Table A7, and able A8 include a scene-wise quantitative

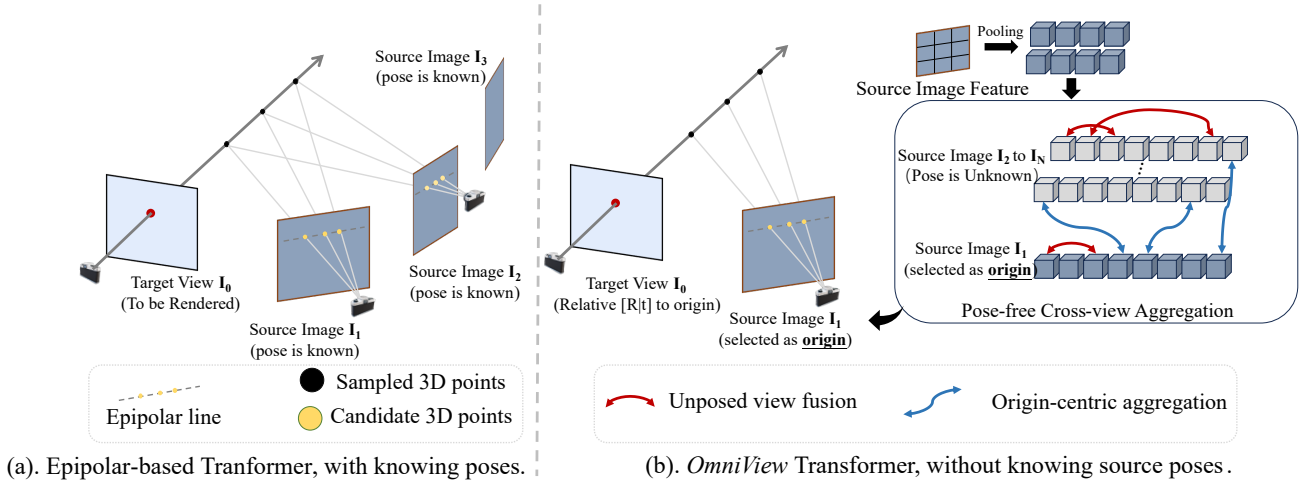


Figure A8. Illustration of *Epipolar Attention* and *OmniView Attention*. The figure is the same with Figure 2 in the main draft.

results presented in the main paper. Our method quantitatively surpasses both the generalizable single-view based method PixelNeRF [48] (and PixelNeRF with finetuning) and multi-view based method UpSRT [31] trained with 4000k iterations and LEAP [17] from the pre-trained model weights. We also include videos to demonstrate our results in the attached video.

**More Free-View Rendering** We provide the visualization of multiple rendered novel viewpoints for the real-world dataset by interpolating between test views. This visualization, illustrated in Figure A9, demonstrates the capabilities of our method in generating diverse viewpoints, offering insight into its performance and potential limitations in real-world scenarios.

## A9. Limitations

Our approach carries certain limitations inherited from these previously proposed methods (e.g., IBRNet [43]). For instance, while our method requires casting rays for rendering a pixel, this inevitably introduces a computational rendering cost, similar to other MLP-based [2, 3, 26] and Transformer-based [36, 40, 43] neural rendering frameworks. Incorporating depth priors from the predictive multi-view depth to guide the point sampling [20], or leveraging the Gaussian Splatting [18] technique may mitigate this efficiency issue.

Table A5. Comparison of PF-GRT with other pose-free generalizable novel view-synthesis methods on the forward-facing LLFF datasets (scene-wise).

Models	Trex	Fern	Flower	Leaves	Room	Fortress	Horns	Orchids
pixelNeRF	8.266	8.655	8.234	7.026	8.872	10.55	7.743	7.177
pixelNeRF-ft	9.6914	9.541	11.9751	7.8957	11.7662	12.729	9.7231	9.2533
SRT	16.383	16.7918	17.0056	14.0108	18.3335	19.7896	16.6579	14.3807
LEAP	8.6914	8.541	10.9751	6.8957	10.7662	11.729	8.7231	8.2533
PF-GRT	21.489	21.847	22.786	17.725	26.836	27.261	23.866	16.139
(a) PSNR $\uparrow$								
Models	Trex	Fern	Flower	Leaves	Room	Fortress	Horns	Orchids
pixelNeRF	0.351	0.326	0.24	0.127	0.492	0.418	0.275	0.161
pixelNeRF-ft	0.3762	0.3639	0.3551	0.1757	0.4983	0.5289	0.3719	0.222
SRT	0.8166	0.7976	0.8637	0.801	0.7821	0.8849	0.6413	0.7349
LEAP	0.2596	0.3175	0.3435	0.4334	0.1388	0.2476	0.352	0.4128
PF-GTR	0.798	0.737	0.773	0.674	0.848	0.820	0.804	0.590
(b) SSIM $\uparrow$								
Models	Trex	Fern	Flower	Leaves	Room	Fortress	Horns	Orchids
pixelNeRF	0.618	0.645	0.658	0.668	0.603	0.582	0.669	0.738
pixelNeRF-ft	0.5496	0.6075	0.6335	0.7234	0.4288	0.5376	0.642	0.7028
SRT	0.3754	0.4158	0.4337	0.5559	0.2397	0.3417	0.4471	0.5375
LEAP	0.6508	0.7514	0.75	0.7542	0.5786	0.7135	0.673	0.7877
PF-GRT	0.181	0.208	0.158	0.285	0.133	0.136	0.171	0.312
(c) LPIPS $\downarrow$								

Table A6. Comparison of PF-GRT with other pose-free generalizable novel view-synthesis methods on the Shiny datasets (scene-wise).

Models	CD	Giants	Lab	Seasoning	Pasta	Crest	Food
pixelNeRF	11.2911	8.7536	10.1085	9.0397	8.7596	8.6769	9.3571
pixelNeRF-ft	12.5323	9.7544	11.0138	9.0327	9.6698	9.3726	10.3788
SRT	15.5747	16.2062	11.7957	15.668	13.5123	12.6199	14.4884
LEAP	10.4334	8.919	9.4274	6.9765	10.9673	9.156	10.15
PF-GRT	23.3704	22.1177	13.561	22.8052	19.1302	14.0699	19.1466
(a) PSNR $\uparrow$							
Models	CD	Giants	Lab	Seasoning	Pasta	Crest	Food
pixelNeRF	0.351	0.326	0.24	0.127	0.492	0.418	0.275
pixelNeRF-ft	0.3762	0.3639	0.3551	0.1757	0.4983	0.5289	0.3719
SRT	0.8166	0.7976	0.8637	0.801	0.7821	0.8849	0.6413
LEAP	0.2596	0.3175	0.3435	0.4334	0.1388	0.2476	0.352
PF-GTR	0.798	0.737	0.773	0.674	0.848	0.820	0.804
(b) SSIM $\uparrow$							
Models	CD	Giants	Lab	Seasoning	Pasta	Crest	Food
pixelNeRF	0.6849	0.5693	0.6756	0.6279	0.6499	0.8021	0.6388
pixelNeRF-ft	0.6628	0.5492	0.6704	0.6265	0.631	0.7897	0.6379
SRT	0.3308	0.2361	0.5706	0.3832	0.2284	0.5667	0.3395
LEAP	0.6449	0.7132	0.6774	0.6807	0.702	0.7294	0.6782
PF-GRT	0.1896	0.2178	0.5078	0.2149	0.187	0.5232	0.2912
(c) LPIPS $\downarrow$							

Table A7. Comparison of PF-GRT with other pose-free generalizable novel view-synthesis methods on the real Real-Estate datasets (scene-wise).

Models	0bcef	000db	000eb	8516c
pixelNeRF	8.541	9.284	10.084	8.055
pixelNeRF-ft	11.5395	11.4856	10.7908	10.5445
SRT	17.1401	17.3898	16.261	16.6377
LEAP	11.6061	12.329	11.3418	11.2685
PF-GRT	24.760	22.808	23.487	25.778

(a) PSNR $\uparrow$

Models	0bcef	000db	000eb	8516c
pixelNeRF	0.427	0.380	0.401	0.373
pixelNeRF-ft	0.5093	0.4646	0.48	0.4381
SRT	0.6594	0.5449	0.5429	0.6012
LEAP	0.528	0.5261	0.5256	0.5291
PF-GRT	0.804	0.750	0.785	0.816

(b) SSIM $\uparrow$

Models	0bcef	000db	000eb	8516c
pixelNeRF	0.507	0.515	0.486	0.504
pixelNeRF-ft	0.4958	0.4694	0.4518	0.5018
SRT	0.3152	0.2922	0.3252	0.3134
LEAP	0.4608	0.4563	0.4408	0.4581
PF-GRT	0.174	0.220	0.193	0.172

(c) LPIPS $\downarrow$

Table A8. Comparison of PF-GRT with other pose-free generalizable novel view-synthesis methods on the NeRF Synthetic Datasets (scene-wise).

Models	Chair	Drums	Ficus	Hotdog	Materials	Mic	Ship	Lego
pixelNeRF	7.2024	7.7479	7.4265	6.9255	7.0926	7.0269	6.3125	7.1134
pixelNeRF-ft	7.8914	8.3051	8.1891	7.6405	8.2315	7.591	7.2083	8.0065
SRT	16.0348	15.6772	15.0571	15.8147	15.1039	14.5086	13.7598	14.417
LEAP	17.466	15.2234	19.4337	17.0554	17.0797	19.4747	21.6511	16.7814
PF-GRT	25.104	19.192	21.785	22.712	27.359	25.14	16.533	21.019
(a) PSNR $\uparrow$								
Models	Chair	Drums	Ficus	Hotdog	Materials	Mic	Ship	Lego
pixelNeRF	0.6046	0.5743	0.6283	0.6036	0.5708	0.6191	0.4011	0.5232
pixelNeRF-ft	0.6435	0.6334	0.68	0.6643	0.6083	0.6564	0.4278	0.5535
SRT	0.8166	0.7976	0.8637	0.801	0.7821	0.8849	0.6413	0.7349
LEAP	0.8696	0.7965	0.9094	0.831	0.8049	0.9089	0.7531	0.7598
PF-GRT	0.871	0.835	0.822	0.875	0.8	0.881	0.677	0.817
(b) SSIM $\uparrow$								
Models	Chair	Drums	Ficus	Hotdog	Materials	Mic	Ship	Lego
pixelNeRF	0.3755	0.4147	0.3515	0.4186	0.4162	0.372	0.5294	0.4321
pixelNeRF-ft	0.3651	0.4076	0.3223	0.3715	0.3819	0.3453	0.5064	0.4018
SRT	0.2024	0.2121	0.1883	0.2318	0.2148	0.1942	0.2787	0.2505
LEAP	0.1666	0.2132	0.1184	0.2169	0.1896	0.1111	0.246	0.2243
PF-GRT	0.083	0.154	0.098	0.087	0.174	0.046	0.402	0.126
(c) LPIPS $\downarrow$								

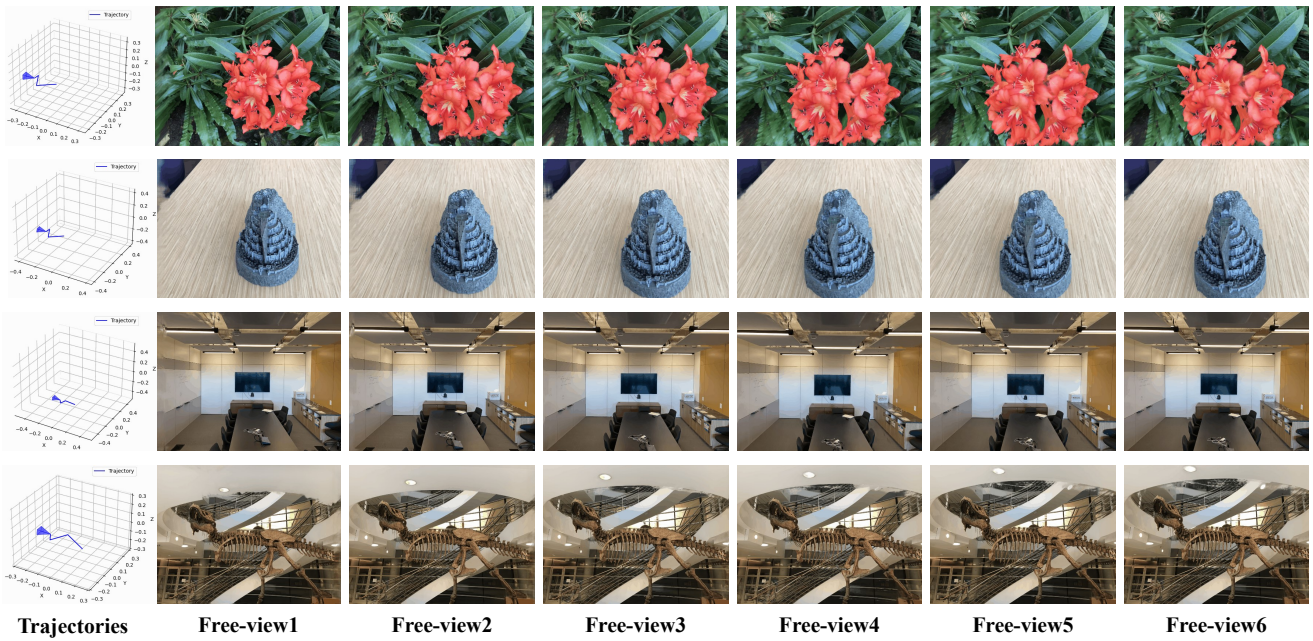


Figure A9. Visualization on more interpolated viewpoints. The visualized images showcase the efficacy of our method in handling various viewpoints by interpolating between test views on real-world datasets. See the video in supplementary materials for more detailed comparisons.

## References

- [1] Benjamin Attal, Jia-Bin Huang, Michael Zollhoefer, Johannes Kopf, and Changil Kim. Learning Neural Light Fields With Ray-Space Embedding Networks. *2022 IEEE/CVF Conference on Computer Vision and Pattern Recognition (CVPR)*, pages 19787–19797, 2022. [2](#)
- [2] Jonathan T Barron, Ben Mildenhall, Matthew Tancik, Peter Hedman, Ricardo Martin-Brualla, and Pratul P Srinivasan. Mip-Nerf: A Multiscale Representation for Anti-Aliasing Neural Radiance Fields. In *Proceedings of the IEEE/CVF International Conference on Computer Vision*, pages 5855–5864, 2021. [A2](#)
- [3] Jonathan T. Barron, Ben Mildenhall, Dor Verbin, Pratul P. Srinivasan, and Peter Hedman. Mip-NeRF 360: Unbounded Anti-Aliased Neural Radiance Fields. *2022 IEEE/CVF Conference on Computer Vision and Pattern Recognition (CVPR)*, pages 5460–5469, 2022. [2](#), [A2](#)
- [4] Wenjing Bian, Zirui Wang, Kejie Li, Jia-Wang Bian, and Victor Adrian Prisacariu. Nope-nerf: Optimising neural radiance field with no pose prior. In *Proceedings of the IEEE/CVF Conference on Computer Vision and Pattern Recognition*, pages 4160–4169, 2023. [3](#)
- [5] Anpei Chen, Zexiang Xu, Fuqiang Zhao, Xiaoshuai Zhang, Fanbo Xiang, Jingyi Yu, and Hao Su. Mvsnerf: Fast Generalizable Field Reconstruction From Multi-View Stereo. In *Proceedings of the IEEE/CVF International Conference on Computer Vision*, pages 14124–14133, 2021. [3](#)
- [6] Shin-Fang Chng, Sameera Ramasinghe, Jamie Sherrah, and Simon Lucey. Garf: gaussian activated radiance fields for high fidelity reconstruction and pose estimation. *arXiv e-prints*, pages arXiv–2204, 2022. [3](#)
- [7] Alexey Dosovitskiy, Lucas Beyer, Alexander Kolesnikov, Dirk Weissenborn, Xiaohua Zhai, Thomas Unterthiner, Mostafa Dehghani, Matthias Minderer, Georg Heigold, Sylvain Gelly, et al. An image is worth 16x16 words: Transformers for image recognition at scale. *arXiv preprint arXiv:2010.11929*, 2020. [A1](#)
- [8] Laura Downs, Anthony Francis, Nate Koenig, Brandon Kinman, Ryan Hickman, Krista Reymann, Thomas B McHugh, and Vincent Vanhoucke. Google scanned objects: A high-quality dataset of 3d scanned household items. In *2022 International Conference on Robotics and Automation (ICRA)*, pages 2553–2560. IEEE, 2022. [6](#)
- [9] Brandon Yushan Feng and Amitabh Varshney. SIGNET: Efficient Neural Representation for Light Fields. *2021 IEEE/CVF International Conference on Computer Vision (ICCV)*, pages 14204–14213, 2021. [2](#)
- [10] John Flynn, Michael Broxton, Paul Debevec, Matthew Duvall, Graham Fyffe, Ryan Overbeck, Noah Snavely, and Richard Tucker. Deepview: View synthesis with learned gradient descent. In *Proceedings of the IEEE/CVF Conference on Computer Vision and Pattern Recognition*, pages 2367–2376, 2019. [6](#)
- [11] Sara Fridovich-Keil, Alex Yu, Matthew Tancik, Qinzhong Chen, Benjamin Recht, and Angjoo Kanazawa. Plenoxels: Radiance Fields Without Neural Networks. In *Proceedings of the IEEE/CVF Conference on Computer Vision and Pattern Recognition*, pages 5501–5510, 2022. [2](#)
- [12] Stephan J Garbin, Marek Kowalski, Matthew Johnson, Jamie Shotton, and Julien Valentin. Fastnerf: High-fidelity neural rendering at 200fps. In *Proceedings of the IEEE/CVF International Conference on Computer Vision*, pages 14346–14355, 2021. [2](#)
- [13] Kaiming He, Xiangyu Zhang, Shaoqing Ren, and Jian Sun. Deep residual learning for image recognition. In *Proceedings of the IEEE conference on computer vision and pattern recognition*, pages 770–778, 2016. [4](#)
- [14] Peter Hedman, Julien Philip, True Price, Jan-Michael Frahm, George Drettakis, and Gabriel Brostow. Deep blending for free-viewpoint image-based rendering. *ACM Transactions on Graphics (ToG)*, 37(6):1–15, 2018. [2](#)
- [15] Peter Hedman, Pratul P Srinivasan, Ben Mildenhall, Jonathan T Barron, and Paul Debevec. Baking neural radiance fields for real-time view synthesis. In *Proceedings of the IEEE/CVF International Conference on Computer Vision*, pages 5875–5884, 2021. [2](#)
- [16] Tao Hu, Shu Liu, Yilun Chen, Tiancheng Shen, and Jiaya Jia. EfficientNeRF Efficient Neural Radiance Fields. In *Proceedings of the IEEE/CVF Conference on Computer Vision and Pattern Recognition*, pages 12902–12911, 2022. [2](#)
- [17] Hanwen Jiang, Zhenyu Jiang, Yue Zhao, and Qixing Huang. Leap: Liberate sparse-view 3d modeling from camera poses. *arXiv preprint arXiv:2310.01410*, 2023. [3](#), [5](#), [6](#), [A2](#)
- [18] Bernhard Kerbl, Georgios Kopanas, Thomas Leimkuehler, and George Drettakis. 3d gaussian splatting for real-time radiance field rendering. *ACM Transactions on Graphics (ToG)*, 42(4):1–14, 2023. [A2](#)
- [19] Chen-Hsuan Lin, Wei-Chiu Ma, Antonio Torralba, and Simon Lucey. Barf: Bundle-adjusting neural radiance fields. In *Proceedings of the IEEE/CVF International Conference on Computer Vision*, pages 5741–5751, 2021. [3](#), [6](#)
- [20] Haotong Lin, Sida Peng, Zhen Xu, Yunzhi Yan, Qing Shuai, Hujun Bao, and Xiaowei Zhou. Efficient neural radiance fields for interactive free-viewpoint video. In *SIGGRAPH Asia 2022 Conference Papers*, pages 1–9, 2022. [A2](#)
- [21] Lingjie Liu, Jiatao Gu, Kyaw Zaw Lin, Tat-Seng Chua, and Christian Theobalt. Neural Sparse Voxel Fields. *Advances in Neural Information Processing Systems*, 33:15651–15663, 2020. [2](#)
- [22] Yuan Liu, Sida Peng, Lingjie Liu, Qianqian Wang, Peng Wang, Christian Theobalt, Xiaowei Zhou, and Wenping Wang. Neural Rays for Occlusion-Aware Image-Based Rendering. In *Proceedings of the IEEE/CVF Conference on Computer Vision and Pattern Recognition*, pages 7824–7833, 2022. [1](#), [3](#), [6](#), [7](#)
- [23] Stephen Lombardi, Tomas Simon, Jason Saragih, Gabriel Schwartz, Andreas Lehrmann, and Yaser Sheikh. Neural volumes: Learning dynamic renderable volumes from images. *arXiv preprint arXiv:1906.07751*, 2019. [2](#)
- [24] Nelson Max. Optical models for direct volume rendering. *IEEE Transactions on Visualization and Computer Graphics*, 1(2):99–108, 1995. [4](#)
- [25] Ben Mildenhall, Pratul P Srinivasan, Rodrigo Ortiz-Cayon, Nima Khademi Kalantari, Ravi Ramamoorthi, Ren Ng, and

- Abhishek Kar. Local light field fusion: Practical view synthesis with prescriptive sampling guidelines. *ACM Transactions on Graphics (TOG)*, 38(4):1–14, 2019. 6, 7
- [26] Ben Mildenhall, Pratul P Srinivasan, Matthew Tancik, Jonathan T Barron, Ravi Ramamoorthi, and Ren Ng. Nerf: Representing scenes as neural radiance fields for view synthesis. *Communications of the ACM*, 65(1):99–106, 2021. 2, 4, 6, 7, A2
- [27] Thomas Müller, Alex Evans, Christoph Schied, and Alexander Keller. Instant neural graphics primitives with a multi-resolution hash encoding. *ACM Transactions on Graphics (ToG)*, 41(4):1–15, 2022. 2
- [28] Ethan Perez, Florian Strub, Harm De Vries, Vincent Dumoulin, and Aaron Courville. Film: Visual reasoning with a general conditioning layer. In *Proceedings of the AAAI conference on artificial intelligence*, 2018. 4
- [29] Christian Reiser, Songyou Peng, Yiyi Liao, and Andreas Geiger. Kilonerf: Speeding Up Neural Radiance Fields With Thousands of Tiny MLPs. In *Proceedings of the IEEE/CVF International Conference on Computer Vision*, pages 14335–14345, 2021. 2
- [30] Jeremy Reizenstein, Roman Shapovalov, Philipp Henzler, Luca Sbordone, Patrick Labatut, and David Novotny. Common objects in 3d: Large-scale learning and evaluation of real-life 3d category reconstruction. In *Proceedings of the IEEE/CVF International Conference on Computer Vision*, pages 10901–10911, 2021. 3
- [31] Mehdi SM Sajjadi, Henning Meyer, Etienne Pot, Urs Bergmann, Klaus Greff, Noha Radwan, Suhani Vora, Mario Lučić, Daniel Duckworth, Alexey Dosovitskiy, et al. Scene representation transformer: Geometry-free novel view synthesis through set-latent scene representations. In *Proceedings of the IEEE/CVF Conference on Computer Vision and Pattern Recognition*, pages 6229–6238, 2022. 1, 3, 5, 6, A2
- [32] Mehdi SM Sajjadi, Aravindh Mahendran, Thomas Kipf, Etienne Pot, Daniel Duckworth, Mario Lučić, and Klaus Greff. Rust: Latent neural scene representations from unposed imagery. In *Proceedings of the IEEE/CVF Conference on Computer Vision and Pattern Recognition*, pages 17297–17306, 2023. 1, 3
- [33] Johannes Lutz Schönberger and Jan-Michael Frahm. Structure-from-Motion Revisited. In *Conference on Computer Vision and Pattern Recognition (CVPR)*, 2016. 1, 6
- [34] Vincent Sitzmann, Semon Rezchikov, William T. Freeman, Joshua B. Tenenbaum, and Frédo Durand. Light Field Networks: Neural Scene Representations With Single-Evaluation Rendering. *Advances in Neural Information Processing Systems*, 34, 2021. 2
- [35] Cameron Smith, Yilun Du, Ayush Tewari, and Vincent Sitzmann. Flowcam: Training generalizable 3d radiance fields without camera poses via pixel-aligned scene flow. *arXiv preprint arXiv:2306.00180*, 2023. 3
- [36] Mohammed Suhail, Carlos Esteves, Leonid Sigal, and Ameesh Makadia. Generalizable patch-based neural rendering. In *European Conference on Computer Vision*, pages 156–174. Springer, 2022. 1, 3, 4, A1, A2
- [37] Mohammed Suhail, Carlos Esteves, Leonid Sigal, and Ameesh Makadia. Light field neural rendering. In *Proceedings of the IEEE/CVF Conference on Computer Vision and Pattern Recognition*, pages 8269–8279, 2022. 3
- [38] Cheng Sun, Min Sun, and Hwann-Tzong Chen. Direct Voxel Grid Optimization: Super-Fast Convergence for Radiance Fields Reconstruction. In *Proceedings of the IEEE/CVF Conference on Computer Vision and Pattern Recognition*, pages 5459–5469, 2022. 2
- [39] Fengrui Tian, Shaoyi Du, and Yueqi Duan. Mononerf: Learning a generalizable dynamic radiance field from monocular videos. *arXiv preprint arXiv:2212.13056*, 2022. 3
- [40] Mukund Varma, Peihao Wang, Xuxi Chen, Tianlong Chen, Subhashini Venugopalan, and Zhangyang Wang. Is attention all that nerf needs? In *The Eleventh International Conference on Learning Representations*, 2022. 1, 3, 4, 6, 7, A1, A2
- [41] Ashish Vaswani, Noam Shazeer, Niki Parmar, Jakob Uszkoreit, Llion Jones, Aidan N Gomez, Łukasz Kaiser, and Illia Polosukhin. Attention is all you need. *Advances in neural information processing systems*, 30, 2017. 2
- [42] Huan Wang, Jian Ren, Zeng Huang, Kyle Olszewski, Menglei Chai, Yun Fu, and S. Tulyakov. R2L: Distilling Neural Radiance Field to Neural Light Field for Efficient Novel View Synthesis. In *European Conference on Computer Vision*. Springer, Springer, 2022. 2
- [43] Qianqian Wang, Zhicheng Wang, Kyle Genova, Pratul P Srinivasan, Howard Zhou, Jonathan T Barron, Ricardo Martin-Brualla, Noah Snively, and Thomas Funkhouser. Ibrnet: Learning multi-view image-based rendering. In *Proceedings of the IEEE/CVF Conference on Computer Vision and Pattern Recognition*, pages 4690–4699, 2021. 1, 2, 3, 6, 7, A2
- [44] Zirui Wang, Shangzhe Wu, Weidi Xie, Min Chen, and Victor Adrian Prisacariu. Nerf-: Neural radiance fields without known camera parameters. *arXiv preprint arXiv:2102.07064*, 2021. 3
- [45] Suttisak Wizatwongsa, Pakkapon Phongthawee, Jiraphon Yenphraphai, and Supasorn Suwajanakorn. Nex: Real-time view synthesis with neural basis expansion. In *Proceedings of the IEEE/CVF Conference on Computer Vision and Pattern Recognition*, pages 8534–8543, 2021. 6
- [46] Tong Wu, Jiarui Zhang, Xiao Fu, Yuxin Wang, Jiawei Ren, Liang Pan, Wayne Wu, Lei Yang, Jiaqi Wang, Chen Qian, et al. Omniobject3d: Large-vocabulary 3d object dataset for realistic perception, reconstruction and generation. In *Proceedings of the IEEE/CVF Conference on Computer Vision and Pattern Recognition*, pages 803–814, 2023. 6
- [47] Alex Yu, Ruilong Li, Matthew Tancik, Hao Li, Ren Ng, and Angjoo Kanazawa. Plenotrees for Real-Time Rendering of Neural Radiance Fields. In *Proceedings of the IEEE/CVF International Conference on Computer Vision*, pages 5752–5761, 2021. 2
- [48] Alex Yu, Vickie Ye, Matthew Tancik, and Angjoo Kanazawa. pixelnerf: Neural radiance fields from one or few images. In *Proceedings of the IEEE/CVF Conference on Computer Vision and Pattern Recognition*, pages 4578–4587, 2021. 1, 3, 5, 6, A2

- [49] Richard Zhang, Phillip Isola, Alexei A Efros, Eli Shechtman, and Oliver Wang. The unreasonable effectiveness of deep features as a perceptual metric. In *Proceedings of the IEEE conference on computer vision and pattern recognition*, pages 586–595, 2018. 6
- [50] Tinghui Zhou, Richard Tucker, John Flynn, Graham Fyffe, and Noah Snavely. Stereo magnification: Learning view synthesis using multiplane images. *arXiv preprint arXiv:1805.09817*, 2018. 6